Predicting Peak Resistance of Spudcan Penetrating Sand Overlying Clay

P. Hu[1]; S. A. Stanier[2]; M. J. Cassidy[3]; and D. Wang[4]

Abstract: Accurately predicting peak penetration resistance q_{peak} during spudcan installation into sand overlying clay is crucial to an offshore mobile jack-up industry still suffering regular punch-through failures. This paper describes a series of spudcan penetration tests performed on medium-loose sand overlying clay and compares the response to existing centrifuge data from tests performed on dense sand overlying clay. Together these data demonstrate that punch-through is a potential problem for both dense and loose sand overlying clay soil stratigraphies. Using this experimental database, a failure-stress-dependent model has been modified to account for the embedment depth, and the depth of occurrence of q_{peak} is shown to be a function of the sand thickness H_s. The model then was recalibrated, taking these findings into account, for a larger range of material properties and ratios of sand thickness to spudcan diameter (H_s/D). Finally, the performance of the modified and recalibrated model is verified by comparing its predictions with those calculated using current guidelines. The comparisons show that the modified model yields more accurate predictions of q_{peak} over the range of H_s/D ratios of practical interest, which when used in practice will potentially mitigate the risk of unexpected punch-through on sand overlying clay stratigraphies. **DOI: 10.1061/(ASCE)GT.1943-5606.0001016.**

Author keywords: Centrifuge modeling; Spudcan; Sand; Clay; Punch-through; Offshore engineering.

Introduction

Modern jack-up structures typically consist of a triangular platform with three legs that are jacked through the deck into the seabed. A jack-up is then installed by filling water ballast tanks on the platform, which pushes the legs and large inverted conical spudcan footings attached at the ends into the seabed soil. This preloading procedure continues until the spudcans have been effectively proof tested, at which time the ballast water is dumped, and the platform is jacked up above the water surface for operation. When jack-up platforms are installed on seabed sediments consisting of a sand layer overlying soft clay, there is the potential for punch-through failure, where the spudcan footing pushes the stronger layer into the softer layer. This can cause vertical displacement of one or more of the legs of the platform in a rapid and uncontrolled manner, which as a consequence can lead to buckling of the legs or in extreme cases even toppling of the platform. The cost of these incidents is estimated to be between US$10 million and US$30 million, and such incidents continue to be problematic (Hossain and Safinus 2012). Therefore, accurately predicting the peak penetration resistance and thus the potential for punch-through failure is an important issue for jack-up platform operators both for operational safety and for field-development economics.

Craig and Chua (1990) performed a series of centrifuge tests investigating the potential for punch-through of foundations on sand overlying clay. They observed that a peak penetration resistance was attained relatively rapidly, which was followed by reducing penetration resistance that caused rapid leg penetration. Cutting of the samples along the central cross section after spudcan extraction exposed a slightly downward-tapering plug of sand with depth approximately equal to the sand-layer height. In contrast, an inverted truncated-cone sand plug was visualized by Teh et al. (2008) using the particle-image velocimetry technique (White et al. 2003) in a centrifuge, and the failure mechanism of spudcan foundations on sand overlying clay was discussed. Teh et al. (2010) proposed that the bearing-resistance–depth profile of a punch-through event can be determined by three characteristic bearing resistances and corresponding depths. Based on an extensive series of flat-footing and spudcan penetration tests on dense sand overlying clay and the observations of Teh et al. (2008), Lee et al. (2013b) proposed a failure stress-dependent model to calculate the peak penetration resistance q_{peak}. However, the model was calibrated solely using experimental data for dense sand overlying clay and for limited geometries of spudcan foundations. Its performance therefore requires further validation. Of greatest concern is whether recalibration is needed for looser sands overlying clay soil conditions.

The aims of this paper are

1. To model experimentally the penetration resistance of a spudcan of generalized geometry penetrating medium-loose sand overlying clay in the centrifuge and to access the potential for punch-through failure;
2. To extend the stress-dependent model for predicting peak penetration resistance of Lee et al. (2013b) to (a) both loose and dense sands and (b) account for the embedment depth of the peak penetration resistance;

[1]Ph.D. Student, Centre for Offshore Foundation Systems, Univ. of Western Australia, Crawley, WA 6009, Australia (corresponding author). E-mail: 20848369@student.uwa.edu.au

[2]Research Associate, Centre for Offshore Foundation Systems, Univ. of Western Australia, Crawley, WA 6009, Australia. E-mail: sam.stanier@uwa.edu.au

[3]Professor, Centre for Offshore Foundation Systems, Univ. of Western Australia, Crawley, WA 6009, Australia. E-mail: mark.cassidy@uwa.edu.au

[4]Assistant Professor, Centre for Offshore Foundation Systems, Univ. of Western Australia, Crawley, WA 6009, Australia. E-mail: dong.wang@uwa.edu.au

Note. This manuscript was submitted on October 4, 2012; approved on July 25, 2013; published online on July 27, 2013. Discussion period open until April 18, 2014; separate discussions must be submitted for individual papers. This paper is part of the ***Journal of Geotechnical and Geoenvironmental Engineering***, © ASCE, ISSN 1090-0241/04013009(12)/$25.00.

3. To recalibrate the modified model based on the experimental results;
4. To investigate the ability of the modified model to predict peak penetration resistance during spudcan foundation installation on sands overlying clay; and
5. To assess the performance of the modified model by comparison with current recommended practices using centrifuge data reported in the literature.

Experimental Setup

Physical modeling of spudcan penetration on medium-loose sand overlying clay was conducted using the drum centrifuge at the University of Western Australia (UWA), a detailed description of which was reported by Stewart et al. (1998). Spudcan foundations in practice are typically circular with diameters of 10–20 m. In this investigation, a generalized-geometry spudcan as illustrated in Fig. 1 was used and was referred to as the UWA spudcan. The spigot angle of 76° and main conical angle of 13° were kept constant for different model spudcan diameters to ensure that any geometric impacts remained consistent between tests. Table 1 contains a summary of the prototype spudcan geometries tested in this investigation. This UWA spudcan was identical to the model spudcan in dense sand overlying clay by Lee et al. (2013a).

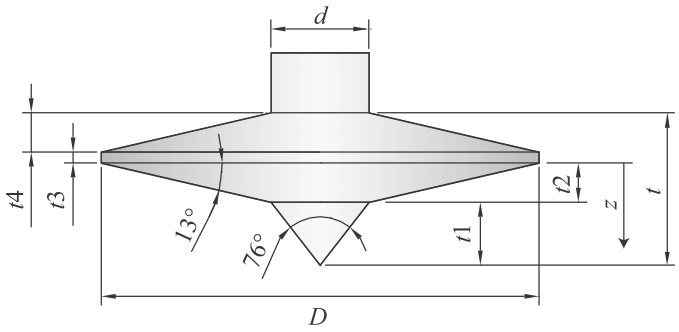

Fig. 1. Generalized UWA spudcan geometry

Commercially available superfine silica sand and kaolin clay were adopted in all the centrifuge tests to form the sand and clay layers, respectively. Both materials have been well characterized and used extensively in the geotechnical centrifuges at UWA. The key properties of the sand and clay are summarized in Cheong (2002) and Stewart (1992), respectively.

The kaolin clay was mixed into a slurry with a water content of 120%. It was then placed in the drum channel using the actuator at an acceleration of 20g until the channel was full before being normally consolidated at an acceleration of 300g. After consolidation, the normally consolidated clay was scraped back, leaving a nonzero shear strength at the sample surface and the desired target clay thickness of 150 mm. A fabric membrane was then placed on top of the clay, and sand was pluviated into the channel under an acceleration of 20g using a specially designed sand placement tool. Medium-loose sand was formed by pluviating the fine particles through a layer of water kept on top of the sample. The underlying clay was then lightly overconsolidated at an acceleration of 300g. The sand and fabric membrane were removed before the sand was laid again following the same procedure but without the fabric membrane. The fabric membrane was used to facilitate removal of the surcharging sand layer, which was disturbed during normal consolidation of the underlying clay layer, allowing relaying of a new, undisturbed sand layer for testing. A target sand thickness was achieved by scraping the sand surface down to the desired height by means of a scraping plate attached to the actuator. All tests were conducted at 200g, and the overconsolidation ratio (OCR) for underlying clay was at least 1.5.

Testing Procedure

Fifteen spudcan penetration tests were performed on medium-loose sand overlying clay with sand thicknesses H_s of 16, 25, and 30 mm. Five tests were conducted at each height, as detailed in Table 1. The ratio of H_s/D was then between 0.16 and 1.0, which covers the range of practical interest because no punch-through failures have been reported for $H_s/D > 1$. The first five tests were performed with a sand thickness of 30 mm. Following these tests, the sand was further scraped back to 25 mm and then to 16 mm (the bottom clay was reconsolidated under 200g overnight after each scraping process), allowing tests to be performed at three sand

Table 1. Relevant Prototype Parameters for Centrifuge Tests in This Investigation

	Geometry						Sand		Clay	
Test name	H_s (m)	D (m)	A (m^2)	H_s/D	d (m)	$t1$, $t2$, $t3$, $t4$ (m)	I_D (%)	γ'_s (kN/m^3)	s_u (kPa)[a]	k (kPa/m)
L1SP1	6	6	28.27	1	2.92	0.86, 0.54, 0.30, 0.35	43	9.96	12.96	1.54
L1SP2	6	8	50.27	0.75	2.92	1.15, 0.72, 0.30, 0.58	43	9.96	12.96	1.54
L1SP3	6	10	78.54	0.6	2.92	1.44, 0.89, 0.30, 0.81	43	9.96	12.96	1.54
L1SP4	6	12	113.10	0.5	2.92	1.73, 1.07, 0.30, 1.07	43	9.96	12.96	1.54
L1SP5	6	14	153.94	0.43	2.92	2.02, 1.25, 0.30, 1.27	43	9.96	12.96	1.54
L2SP1	5	6	28.27	0.83	2.92	0.86, 0.54, 0.30, 0.35	43	9.96	12.36	1.54
L2SP2	5	10	78.54	0.5	2.92	1.44, 0.89, 0.30, 0.81	43	9.96	12.36	1.54
L2SP3	5	14	153.94	0.36	2.92	2.02, 1.25, 0.30, 1.27	43	9.96	12.36	1.54
L2SP4	5	16	201.06	0.31	2.92	2.30, 1.43, 0.30, 1.50	43	9.96	12.36	1.54
L2SP5	5	20	314.16	0.25	2.92	2.88, 1.79, 0.30, 1.96	43	9.96	12.36	1.54
L3SP1	3.2	6	28.27	0.53	2.92	0.86, 0.54, 0.30, 0.35	43	9.96	11.01	1.55
L3SP2	3.2	8	50.27	0.4	2.92	1.15, 0.72, 0.30, 0.58	43	9.96	11.01	1.55
L3SP3	3.2	12	113.10	0.27	2.92	1.73, 1.07, 0.30, 1.07	43	9.96	11.01	1.55
L3SP4	3.2	16	201.06	0.2	2.92	2.30, 1.43, 0.30, 1.50	43	9.96	11.01	1.55
L3SP5	3.2	20	314.16	0.16	2.92	2.88, 1.79, 0.30, 1.96	43	9.96	11.01	1.55

[a] s_u is from sand-clay interface.

thicknesses. At each stage, the sand was removed over the entire drum channel, but the tests were conducted in different and untouched sites.

The relative density I_D of the sand layer was determined by extracting four samples from equidistant radial locations in the channel using 60-mm-diameter sampling tubes after surcharging and before the tests (at 1g). The samples were collected from the bed carefully, ensuring minimal disturbance, and yielded an average relative density of 43% with a SD of 7%, indicating relatively uniform medium-loose sand. The submerged unit weight of the sand γ'_s was found to be 10.0 kN/m^3. The submerged unit weight of the clay γ'_c was measured directly on 20-mm-diameter samples extracted by a tube sampler and was found to be 7.1 kN/m^3 on average.

The spudcans were loaded using displacement control at a constant penetration rate. The penetration rates were determined such that drained behavior in sand and undrained behavior in clay were attained. The following normalized penetration rate V was widely adopted to describe the drainage condition (Finnie and Randolph 1994):

$$V = \frac{vD}{c_v} \tag{1}$$

where v = penetration velocity of foundation; D = foundation diameter; and c_v = consolidation coefficient. For undrained conditions in clay, there is a transition range of $30 < V < 300$ over which partial drainage is minimized (Finnie and Randolph 1994). The dimensionless velocity V was maintained as 120 in the clay [$c_v = 2$ m^2/year (Stewart 1992)] for all tests by varying the penetration velocity accordingly. Thus the penetration velocities v for $D = 30$ and 100 mm were 0.254 and 0.076 mm/s, respectively. Silica sand has been estimated to have a c_v of at least 60,000 m^2/year (Lee et al. 2013a), and therefore, V was less than 0.01 in the sand layer for the penetration rates and spudcan sizes used. This ensured fully drained behavior in the sand layer.

To obtain the undrained shear-strength profile of clay layer, T-bar penetrometer tests were performed on the clay layer in isolation following careful removal of the upper sand layer after all the spudcan penetration tests had been completed. This was intended to eliminate the influence of entrapped sand beneath the penetrometer and avoid potential damage to the penetrometer that may have occurred if it penetrated through the sand layer. An intermediate roughness T-bar factor of 10.5 was assumed. Given that the OCR increased as the sand was scraped away at intervals during the test schedule to allow for thinner sand thickness, the shear-strength profile of clay measured with the sand removed was calculated using the following relationship to account for the impact of changes in OCR on the shear strength (Koutsoftas and Ladd 1985):

$$\frac{s_u}{\sigma'_v} = a\mathrm{OCR}^b \tag{2}$$

where s_u = undrained shear strength; σ'_v = vertical effective stress; and a and b = fitting parameters. Two example T-bar tests from different locations within the drum channel are presented in Fig. 2, indicating excellent sample uniformity. The OCR profiles for each of the three layer heights were calculated using the measured effective unit weights of the sand and clay layers, prototype dimensions, and the consolidation g level. The best fit of Eq. (2) to the T-bar penetrometer profiles for all three sand-layer heights tested was found with values for a and b of 0.16 and 0.74, respectively. Thus the sand-clay interface shear strengths and shear-strength gradients for the underlying clay layers tested were estimated using linear best fits to the nonlinear profiles estimated using Eq. (2) and are summarized in Table 1. In the following, all experimental results are reported with prototype dimensions.

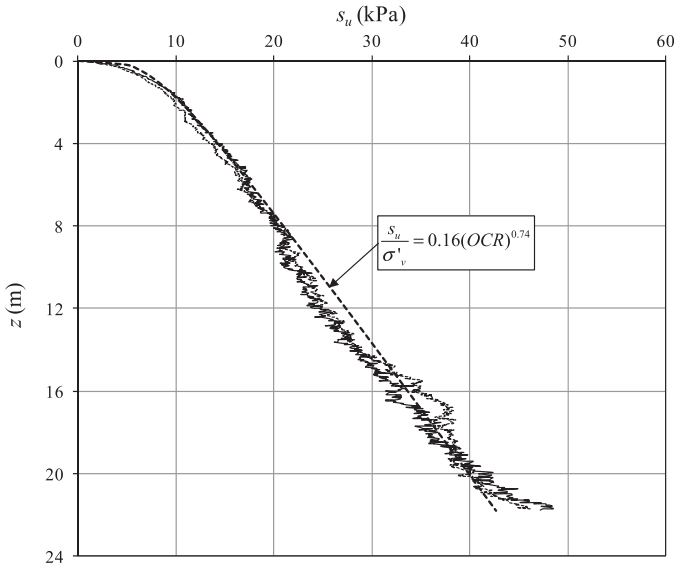

Fig. 2. Shear-strength profile from two T-bar penetration tests ($N_{\text{T-bar}} = 10.5$) demonstrating sample uniformity

Results and Discussion

Penetration Resistance Profiles

The nominal penetration resistance q_{nom} profiles (penetration force normalized by the maximum bearing area of the spudcan) for 15 medium-loose sand overlying clay centrifuge tests are shown in Fig. 3. They are grouped for different sand thicknesses. The displacement measurements are zeroed on full embedment of the bottom shoulder (i.e., spudcan embedded until a depth measured from the tip of the spigot equals $t1 + t2$, given in Table 1), as illustrated in Fig. 1. In general, the potential for both punch-through and rapid leg run (see Fig. 3) is observed in these nominal penetration resistance profiles, indicating a potential risk for spudcan installation on this type of soil stratigraphy. Punch-through and rapid leg run might occur when there is a rapid vertical spudcan displacement. For the case of punch-through, this is the result of an obvious reduction in the penetration resistance profile, whereas for rapid leg run, the rapid displacement may stem from a period of nearly constant q_{peak} in the penetration resistance profile. Generally, punch-through is more likely to occur for larger H_s/D ratios, and rapid leg run is more likely to occur for lower ratios of H_s/D. Rapid leg run is potentially just as dangerous as punch-through because the uncontrolled displacements shown here are as large as 0.3–0.7D.

Fig. 4 presents selected typical nominal penetration resistance profiles for two pairs of spudcan penetration tests on dense and medium-loose sand overlying clay [noting that the $I_D = 92\%$ cases presented is based on the data of Lee (2009)]. These profiles have been chosen because Figs. 4(a and c) and 4(b and d) exhibit identical D values, very similar H_s values, and consequently, very close values of H_s/D. Comparison of these penetration resistance profiles provides insight into the impact of various parameters on the peak penetration resistance and potential for hazardous failure.

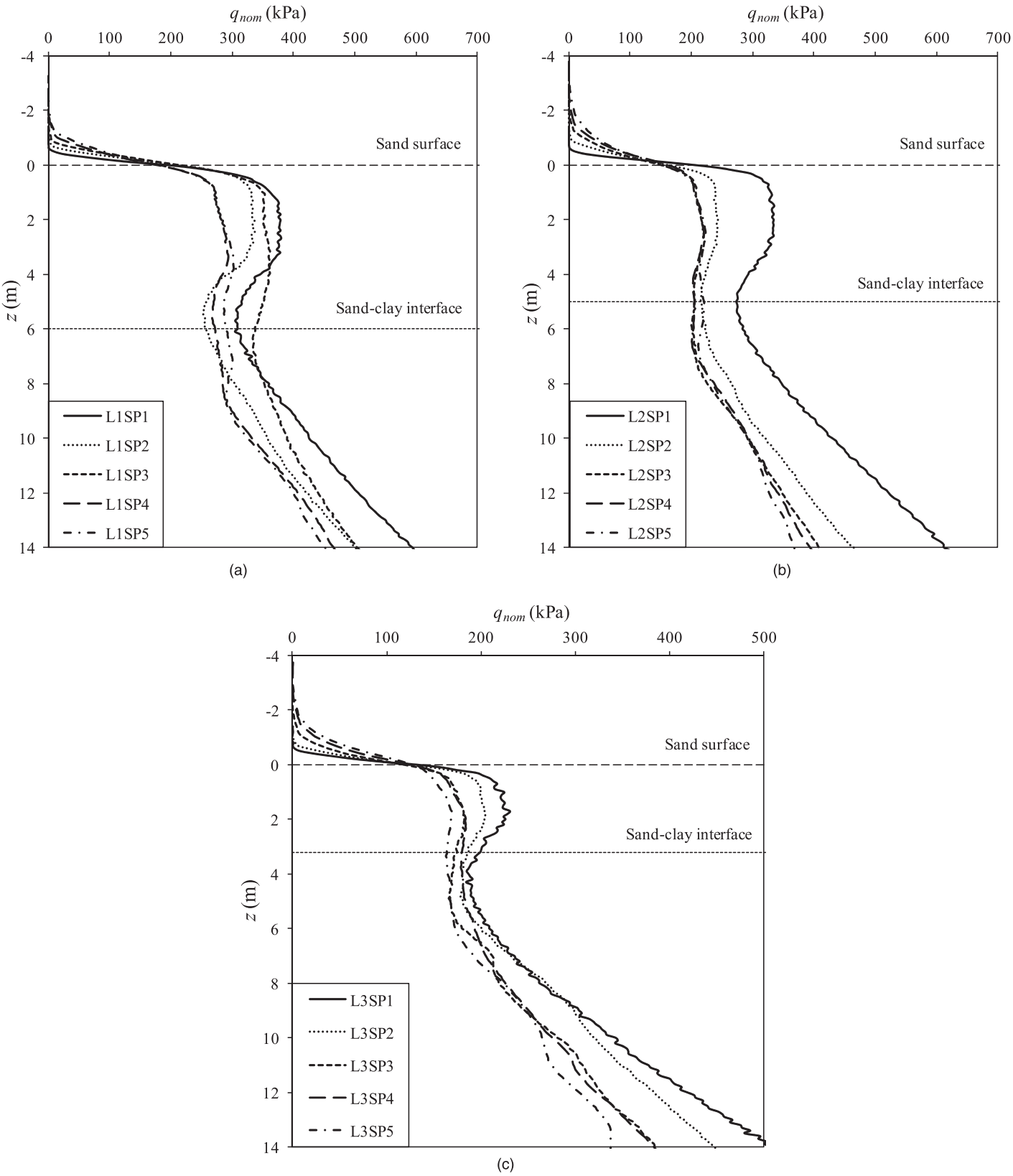

Fig. 3. Penetration resistance profiles for 15 medium-loose sand tests: (a) 6-m sand-layer thickness; (b) 5-m sand-layer thickness; (c) 3.2-m sand-layer thickness

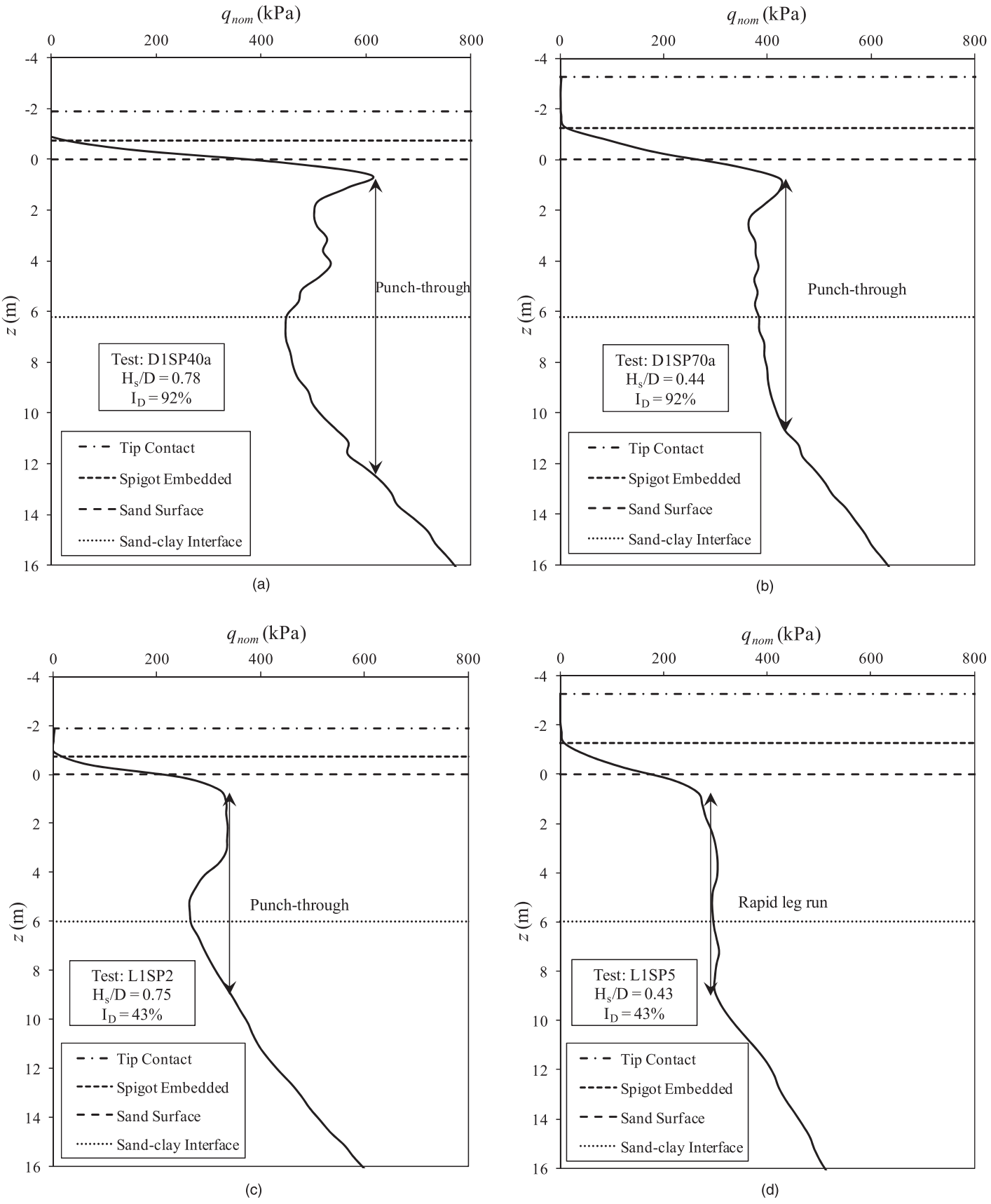

Fig. 4. Typical penetration resistance profiles for dense and medium-loose sand with comparable H_s/D ratios (data for dense sand from Lee 2009): (a) Test D1SP40a ($H_s/D = 0.78$; $I_D = 92\%$); (b) Test D1SP70a ($H_s/D = 0.44$; $I_D = 92\%$); (c) Test L1SP2 ($H_s/D = 0.75$; $I_D = 43\%$); (d) Test L1SP5 ($H_s/D = 0.43$; $I_D = 43\%$)

The comparisons of Figs. 4(a and b) and 4(c and d) demonstrate the impact of H_s/D ratio on the nominal penetration resistance profiles. For both dense and loose sands, q_{peak} reduces with H_s/D ratio. For dense sand with $H_s/D = 0.78$, q_{peak} is 620 kPa, whereas it is 430 kPa for $H_s/D = 0.44$. The reduction in q_{peak} for medium-loose sand is not so obvious but still has a value of 15% for $H_s/D = 0.43$ compared with $H_s/D = 0.75$. This is so because during the mobilization of q_{peak}, for high H_s/D ratios, the influence zone is confined mainly to the sand layer, which would contribute to a large q_{peak}. For the dense sand tests in Figs. 4(a and b), the reduction in H_s/D ratio decreases the magnitude of the peak penetration resistance q_{peak} and also the potential length of the uncontrolled vertical displacement. For the medium-loose sand tests in Figs. 4(c and d), the impact of reducing the H_s/D ratio is to change the potential for failure from punch-through to rapid leg run. This is further confirmed by the other medium-loose sand tests presented in Fig. 3.

Comparison of Figs. 4(a and c) and 4(b and d) highlights the impact of I_D on the failure mode. For high H_s/D ratios, in Figs. 4(a and c), reducing the I_D changes the penetration resistance from a peaked and sudden failure, with significant rapid postpeak resistance reduction, to a more progressive failure with attenuated postpeak resistance reduction. For low H_s/D ratios, in Figs. 4(b and d), the same trend is evident except that the medium-loose sand failure potential becomes a rapid leg run rather than punch-through.

This indicates that punch-through or rapid-leg-run failure is a potential problem for sand overlying clay stratigraphies involving sand from medium-loose to dense states because even in Fig. 4(d), which exhibits the smallest q_{peak}, the potential for uncontrolled rapid leg run was observed. As a result, the failure-stress-dependent model proposed by Lee et al. (2013b) for dense sand overlying clay is developed in this paper to accurately predict q_{peak} for problems involving sand from medium-loose to dense states.

Peak Penetration Resistance

Fig. 5 presents the peak penetration resistance q_{peak} versus the widest cross-sectional area for each of the spudcans tested. The data are grouped in accordance with the thickness and relative density of the sand layer. The figure illustrates that the general variations in the peak penetration resistances with the widest cross-sectional areas may be fitted with power-law equations. Specific equations are not given for these fits because they are only intended to demonstrate trends in the results.

The bearing capacities of the spudcan for modern jack-ups are reported to be in the range of 200–600 kPa (Osborne et al. 2008). The experimentally measured peak penetration resistances shown in Fig. 5 are within this range, which suggests that the current centrifuge model tests were appropriately scaled to calibrate the proposed failure-stress-dependent model.

Depth of Peak Penetration Resistance

In addition to the peak penetration resistance q_{peak}, the depth at which the peak penetration resistance occurs must be predicted because both are necessary for providing a full penetration resistance profile for spudcan penetration on sand overlying clay. Based on centrifuge tests on dense sand overlying clay conducted at UWA and at the National University of Singapore (NUS), Teh et al. (2010) proposed that the effective sand thickness H_{eff} at mobilization of q_{peak} was equal to $0.88H_s$. The depth of penetration required to mobilize the peak penetration resistance d_{peak} ($d_{peak} = H_s - H_{eff}$) is therefore $0.12H_s$. Fig. 6 is a summary of the correlation between H_{eff}/D and H_s/D ratio for all the centrifuge tests listed in Tables 1 and 2 except the beam centrifuge test of Lee (2009), for which the penetration resistance profiles were not available. The relationship proposed by Teh et al. (2010) is consistent for both UWA and NUS geometries of spudcans and the soil properties reported in Tables 1 and 2. Thus the depth of peak penetration resistance relative to the lowest elevation of the spudcan's widest cross-sectional area may be expressed with confidence as

$$d_{peak} = 0.12H_s \tag{3}$$

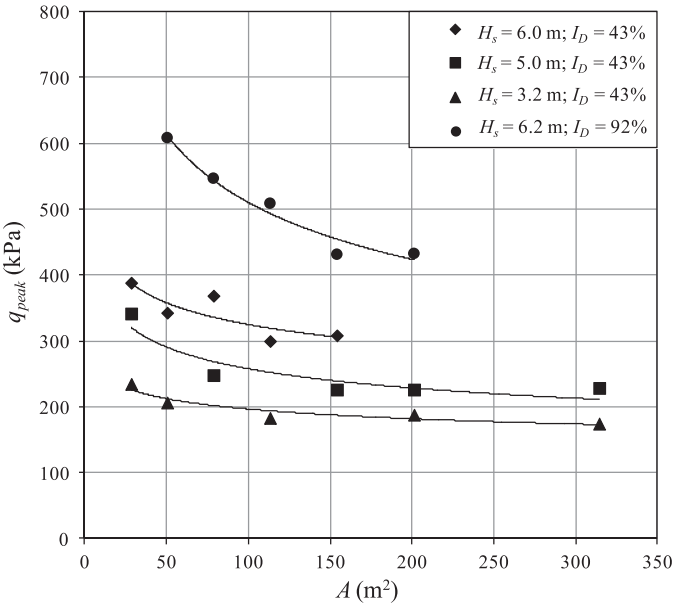

Fig. 5. Peak penetration resistance as a function of the widest cross-sectional area of spudcan [data with $I_D = 92\%$ from Lee (2009)]

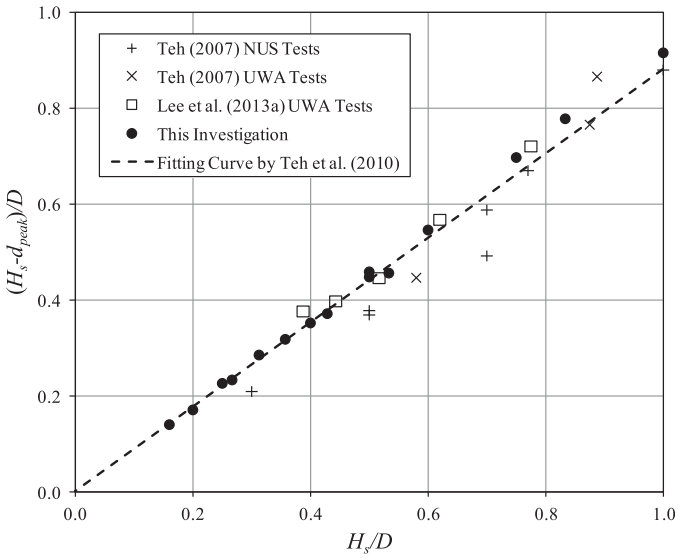

Fig. 6. Correlation between H_{eff}/D and the normalized sand thickness H_s/D

Table 2. Relevant Parameters for Centrifuge Tests from the Literature Used in the Comparative Prediction Performance Study

		Geometry			Sand		Clay	
Investigation	Test name	H_s (m)	D (m)	H_s/D	I_D (%)	γ_s' (kN/m^3)	s_u (kPa)	k (kPa/m)
Teh (2007) NUS tests	NUS_F1	3.0	10	0.30	95	9.93	7.75	1.56
	NUS_F2	5.0	10	0.50	88	9.78	12.71	1.56
	NUS_F3	7.0	10	0.70	94	9.91	18.04	1.56
	NUS_F4	7.7	10	0.77	94	9.90	19.82	1.56
	NUS_F5	10.0	10	1.00	95	9.93	25.82	1.56
	NUS_F8	5.0	10	0.50	61	9.21	11.98	1.56
	NUS_F9	7.0	10	0.70	58	9.15	16.66	1.56
Teh (2007) UWA tests	UWA_F3	3.5	4	0.88	99	11.15	7.22	1.20
	UWA_F4	3.5	6	0.58	99	11.15	7.22	1.20
	UWA_F10	7.1	8	0.89	98	11.13	14.62	1.20
Lee (2009) drum centrifuge tests	D1SP40a	6.2	8	0.78	92	10.99	17.70	2.00
	D1SP50a	6.2	10	0.62	92	10.99	17.70	2.00
	D1SP60a	6.2	12	0.52	92	10.99	17.70	2.00
	D1SP70a	6.2	14	0.44	92	10.99	17.70	2.00
	D1SP80a	6.2	16	0.39	92	10.99	17.70	2.00
Lee (2009) beam centrifuge tests	B1S7SP8a	7.0	8	0.88	99	11.15	13.20	1.85
	B1S7SP8b	7.0	8	0.88	99	11.15	13.20	1.85
	B1S7SP8c	7.0	8	0.88	99	11.15	13.20	1.85
	B1S7SP14a	7.0	14	0.50	99	11.15	13.20	1.85
	B1S7SP14b	7.0	14	0.50	99	11.15	13.20	1.85

Failure-Stress-Dependent Prediction Model

Performance of Original Failure-Stress-Dependent Model

As shown in Fig. 7, Lee et al. (2013b) proposed an analytical model that assumes that the peak penetration resistance occurs when a sand frustrum with a dispersion angle (the angle between the assumed slip surface and the vertical plane) equal to the angle of dilation ψ is pushed into the underlying clay. Hence q_{peak} is the sum of the frictional resistance in the sand, the bearing capacity of the underlying clay, and the weight of the sand frustrum. The operative friction and dilation angles are related to q_{peak} using a modified form of Bolton's (1986) empirical relationships, i.e.,

$$I_R = I_D\left[Q - \ln\left(p'\right)\right] - 1 \quad 0 < I_R < 4 \tag{4}$$

$$\phi' - \phi_{cv} = mI_R \tag{5}$$

$$0.8\psi = \phi' - \phi_{cv} \tag{6}$$

where I_R = dilatancy indicator in degrees; Q = natural logarithm of the grain crushing strength expressed in kilopascals; p' = mean effective stress; ϕ' = operative friction angle; ϕ_{cv} = critical-state friction angle; and m = a constant. Lee et al. (2013a) used 25 centrifuge model tests on dense sand overlying clay and accompanying small-strain finite-element simulations to back-analyze a best-fit value for m of 2.65. The authors also performed similar simulations of the medium-loose sand overlying clay tests presented in this paper with good comparability with the experimental measurements, providing confidence that a value for m of 2.65 was appropriate irrespective of the relative density of the sand layer.

In Lee's analytical model, a distribution factor D_F is defined to relate the local stress along the failure surface to the average vertical stress or, more specifically, the ratio of the vertical effective stress at the slip surface to the mean vertical effective stress. The distribution factor depends on the H_s/D ratio of flat or spudcan foundations, and bilinear equations were proposed to depict the preceding relationship.

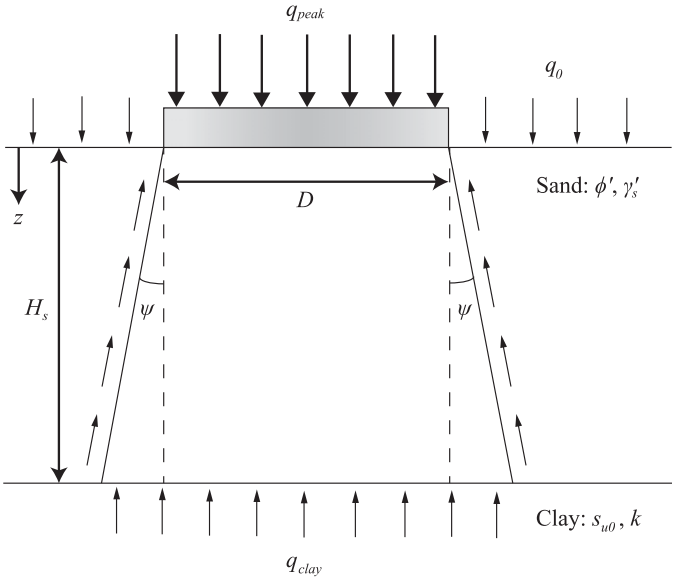

Fig. 7. Failure-stress-dependent mechanism (data from Lee et al. 2013b)

For current tests for medium-loose sand layers, optimized D_F values were derived by varying D_F until the q_{peak} predicted by the original model of Lee et al. (2013b) was equal to the measured value. The optimized D_F values are plotted against H_s/D ratio in Fig. 8(a) alongside the calculated resistance divided by the experimental resistance ($q_{\text{peak, calculated}}/q_{\text{peak, measured}}$) in Fig. 8(b). The bilinear variations in D_F with H_s/D ratio suggested by Lee et al. (2013b) are plotted in Fig. 8 as well. Some skew of the regression line is evident in Fig. 8(b), particularly with smaller H_s/D ratios, which means that

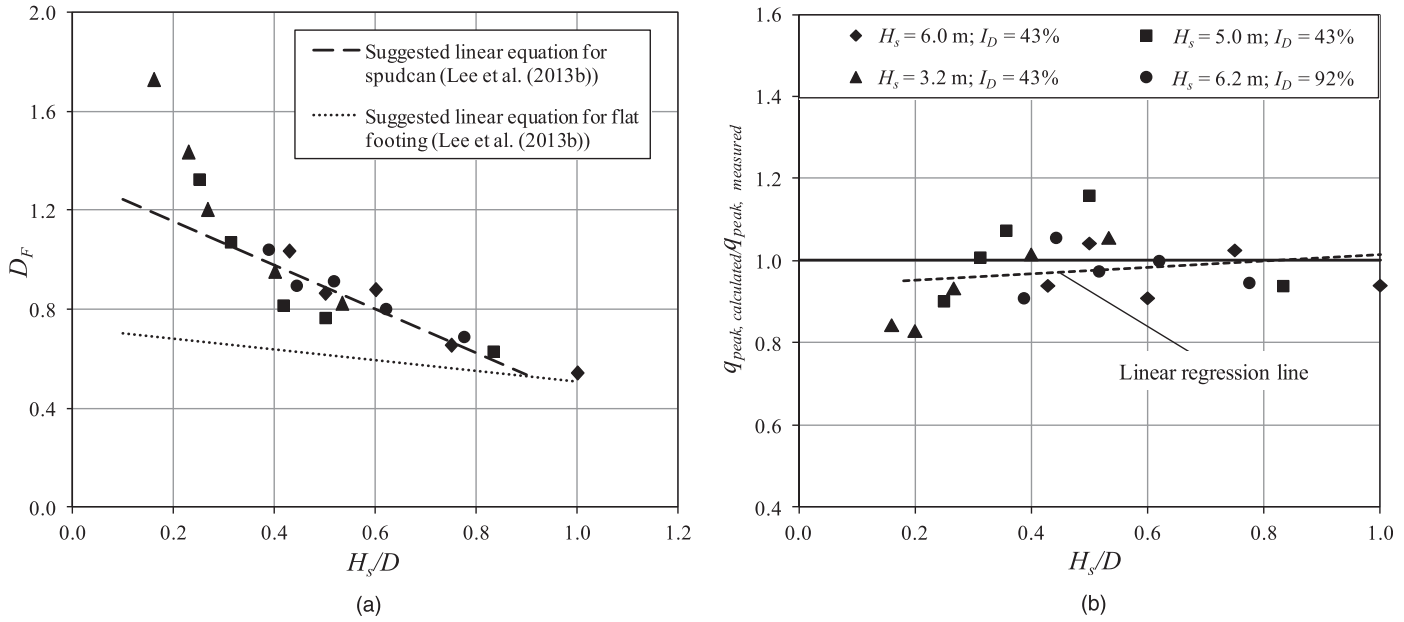

Fig. 8. Performance of Lee's failure-stress-dependent model: (a) calibrated D_F and bilinear relationship equations; (b) predictions based on the model

the original model underestimates the peak penetration reisistance for smaller H_s/D ratios. This is further verified by Fig. 8(a) because the bilinear D_F equations do not capture the trend well, especially for cases where $H_s/D < 0.3$. This is not unexpected because the preceding failure mechanism and bilinear D_F equations in their original state were calibrated solely using experimental data for spudcans in a single height ($H_s = 6.2$ m) of dense sand ($I_D = 92\%$) overlying clay. The original mechanism was validated, and not calibrated, using data from only three tests performed on loose sand overlying clay reported in the literature. In addition, the embedment depth achieved during mobilization of q_{peak} is not accounted for.

Modification of the Failure-Stress-Dependent Model

To account for the embedment depth at failure, the original mechanism was modified as shown in Fig. 9. In this modified failure mechanism, the peak penetration resistance is derived following the same procedure as in Lee et al. (2013b), but the embedment depth attained during mobilization of q_{peak} is taken into account. The D_F values are optimized, and a new power relationship with H_s/D ratio is proposed based on the modified failure mechanism. In brief, the problem is treated mathematically as a series of infinitesimally thin horizontal disks, which allows the following differential equation to be formulated:

$$\frac{\partial \overline{\sigma'_z}}{\partial z} + \frac{E \tan\psi}{(D/2 + z\tan\psi)}\overline{\sigma'_z} - \gamma'_s = 0 \tag{7}$$

where $\overline{\sigma'_z}$ = average vertical stress in each horizontal disk at depth z. The parameter E is adopted to simplify the algebra and taken as

$$E = 2\left[1 + D_F\left(\frac{\tan\phi^*}{\tan\psi} - 1\right)\right] \tag{8}$$

where ϕ^* = reduced friction angle caused by nonassociated flow, which can be expressed as (Drescher and Detournay 1993)

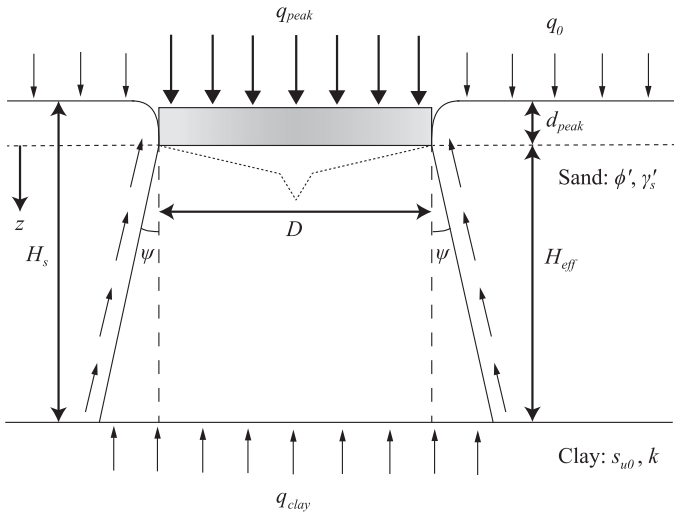

Fig. 9. Modified failure-stress-dependent mechanism accounting for embedment depth attained during mobilization of q_{peak}

$$\tan\phi^* = \frac{\sin\phi' \cos\psi}{1 - \sin\phi' \sin\psi} \tag{9}$$

By assuming that D_F is constant with depth, Eq. (7) can be integrated to give

$$\left(\frac{D}{2} + z\tan\psi\right)^E \cdot \overline{\sigma'_z} = \frac{\gamma'_s\left(\frac{D}{2} + z\tan\psi\right)^{E+1}}{\tan\psi(E+1)} + C \tag{10}$$

where C = a constant that can be determined through the following critical condition. Referring to the conceptual model in Fig. 9, when the depth z is equal to the effective sand thickness H_{eff}, the mean vertical effective stress is equal to the bearing capacity of the underlying clay layer; thus C can be expressed as

J. Geotech. Geoenviron. Eng., 2014, 140(2): 04013009

$$C = \left(\frac{D}{2} + H_{\text{eff}} \tan\psi\right)^E \left[\left(N_{c0}s_{u0} + q_0 + \gamma'_s H_{\text{eff}} + \gamma'_s d_{\text{peak}}\right) - \frac{\gamma'_s\left(\frac{D}{2} + H_{\text{eff}} \tan\psi\right)}{\tan\psi(E+1)}\right] \tag{11}$$

where N_{c0} = bearing-capacity factor of clay at foundation base, which is obtained using the relationship proposed by Houlsby and Martin (2003) for circular foundations with shear strength increasing linearly with depth; s_{u0} = undrained shear strength of the clay at the sand-clay interface; and q_0 = effective overburden pressure at the depth of the foundation.

By substituting Eq. (11) into Eq. (10), the mean vertical effective stress can be expressed as

$$\overline{\sigma'_z} = \frac{\gamma'_s\left(\frac{D}{2} + z\tan\psi\right)}{\tan\psi(E+1)} + \frac{\left(\frac{D}{2} + H_{\text{eff}}\tan\psi\right)^E}{\left(\frac{D}{2} + z\tan\psi\right)^E} \times \left[\left(N_{c_0}s_{u_0} + q_0 + \gamma'_s H_{\text{eff}} + \gamma'_s d_{\text{peak}}\right) - \frac{\gamma'_s\left(\frac{D}{2} + H_{\text{eff}}\tan\psi\right)}{\tan\psi(E+1)}\right] \tag{12}$$

According to Fig. 9, the spudcan penetration depth z is measured from the depth where the peak penetration resistance occurs, and the peak penetration resistance can be obtained by setting z equal to zero. As discussed earlier, $H_{\text{eff}} = 0.88H_s$ for both tests involving dense and loose sand layers, and by substituting $\overline{\sigma'_z}$ with q_{peak} and inputting the values for d_{peak} and H_{eff} into Eq. (12), the peak penetration resistance is thus expressed in terms of H_s.

$$q_{\text{peak}} = \left(N_{c0}s_{u0} + q_0 + 0.12\gamma'_s H_s\right)\left(1 + \frac{1.76H_s}{D}\tan\psi\right)^E + \frac{\gamma'_s D}{2\tan\psi(E+1)}\left[1 - \left(1 - \frac{1.76H_s}{D}E\tan\psi\right) \times \left(1 + \frac{1.76H_s}{D}\tan\psi\right)^E\right] \tag{13}$$

for cases where $\phi' > \phi_{cv}$. Similarly, for cases where $\phi' = \phi_{\text{cv}}$, the peak penetration resistance can be calculated as

$$q_{\text{peak}} = \left(N_{c0}s_{u0} + q_0 + 0.12\gamma'_s H_s\right)e^{E_0} + 0.88\gamma'_s H_s\left[e^{E_0}\left(1 - \frac{1}{E_0}\right) + \frac{1}{E_0}\right] \tag{14}$$

where E_0 is equal to

$$E_0 = 3.52D_F \sin\phi_{cv}\frac{H_s}{D} \tag{15}$$

In Eq. (4), the mean effective stress p' is substituted with q_{peak} in Eq. (13), and through an iterative procedure using Eqs. (4)–(6) and (13) in a spreadsheet analysis (e.g., in Microsoft Excel), this approach allows the operative friction angle and dilatancy (and thus dispersion angle of the sand frustum) to be related to the stress level at failure rather than to the initial state. This method is advantageous because it avoids the use of design charts, and sensitivity analysis can be conducted with ease.

Based on the modified failure-stress-dependent model and with the benefit of the additional experimental data presented, the distribution factor was recalibrated and optimized in terms of a wide range of spudcan geometries and soil conditions incorporating both loose and dense sand overlying clay. The optimized D_F for the additional 15 centrifuge tests for medium-loose sand and tests for the dense sand by Lee (2009) are presented in Fig. 10(a). It is observed that the relationship between D_F and H_s/D ratio is nonlinear and better fitted with the power law.

$$D_F = 0.642\left(\frac{H_s}{D}\right)^{-0.576} \quad \text{as} \quad 0.16 \le \frac{H_s}{D} \le 1.0 \tag{16}$$

Using the original model and the linear relationships proposed by Lee et al. (2013b), the coefficient of determination R^2 is 0.77 for the experimental data in Fig. 10, whereas $R^2 = 0.94$ using the modified model and the power relationship in Eq. (16). For low H_s/D ratios, the embedded volume of the spudcan during mobilization of q_{peak} is a far larger proportion of the volume of the inverted truncated cone in the modified failure mechanism than that for high H_s/D ratios. This embedded volume causes increasing lateral stress and then the larger values of D_F. The embedded volume of the spudcan also can be expressed in terms of H_s/D ratio using a similar power relationship. Although it is not possible to link D_F directly to the embedded volume of the spudcan at q_{peak} (given that the increase in mean stress at the failure surface of the proposed failure mechanism is highly unlikely to be directly proportional to the volume of sand displaced during spudcan embedment), the similar power relationship would suggest that the nonlinear relationship proposed in Eq. (16) to describe D_F for spudcans is logical.

Similar to Fig. 8(b), the scattered markers in Fig. 10(b) show the predictions for both loose and dense sand tests based on the modified mechanism and power relationship of D_F. There is reduced skew for the whole range of H_s/D ratios of practical interest. This is so because the embedment depth during the mobilization of peak penetration resistance is accounted for in the modified failure mechanism, and the new D_F relationship is calibrated for a larger range of spudcan diameters and soil properties. More tests are needed to investigate the suitability of the D_F relationship for different spudcan shapes (conical angles).

Performance of the Modified Model in Predicting q_{peak}

To further validate the performance of the modified and recalibrated model, three series of additional centrifuge test data for the penetration of spudcans into sand overlying normally or lightly overconsolidated clay have been compared. These additional tests consist of seven tests by Teh (2007) in the NUS centrifuge, three tests by Teh (2007) in the UWA beam centrifuge, and five tests by Lee (2009) in the UWA beam centrifuge. Tables 1 and 2 contain a summary of the relevant geometric and material parameters of these tests, as well as the experimental results. All the data used in

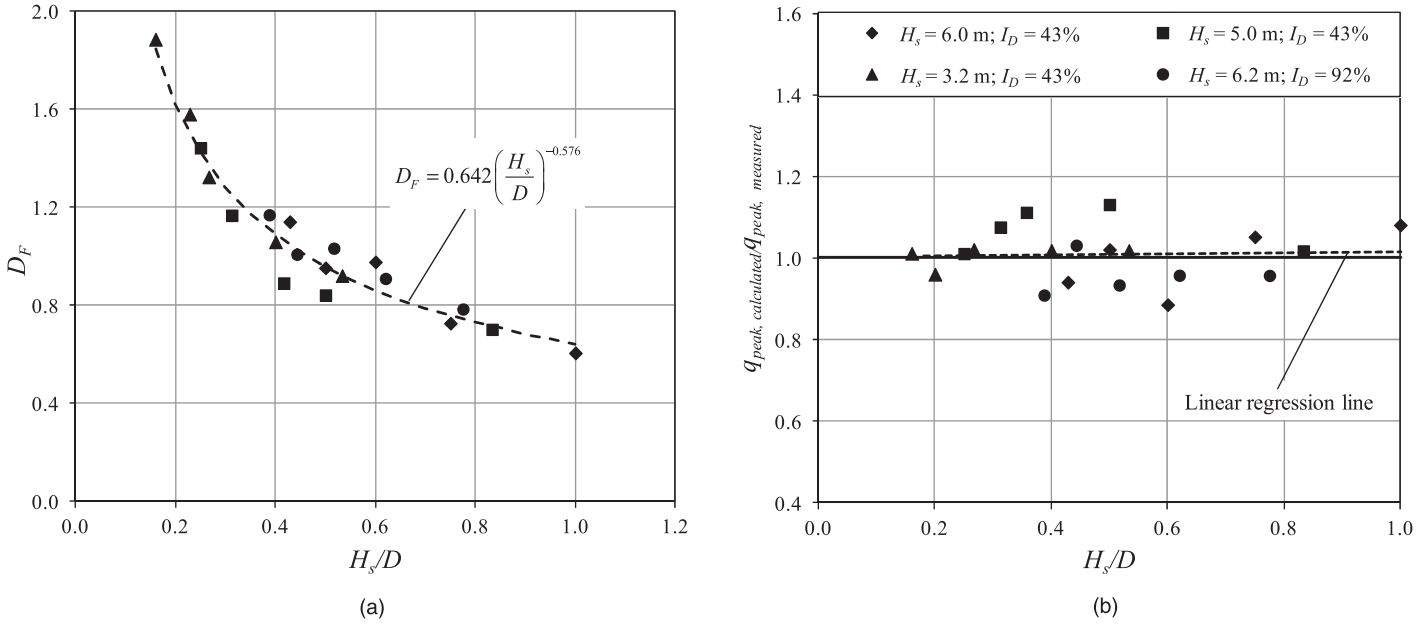

Fig. 10. Performance of modified failure-stress-dependent model: (a) calibrated D_F and nonlinear relationship equation; (b) predictions based on the modified model

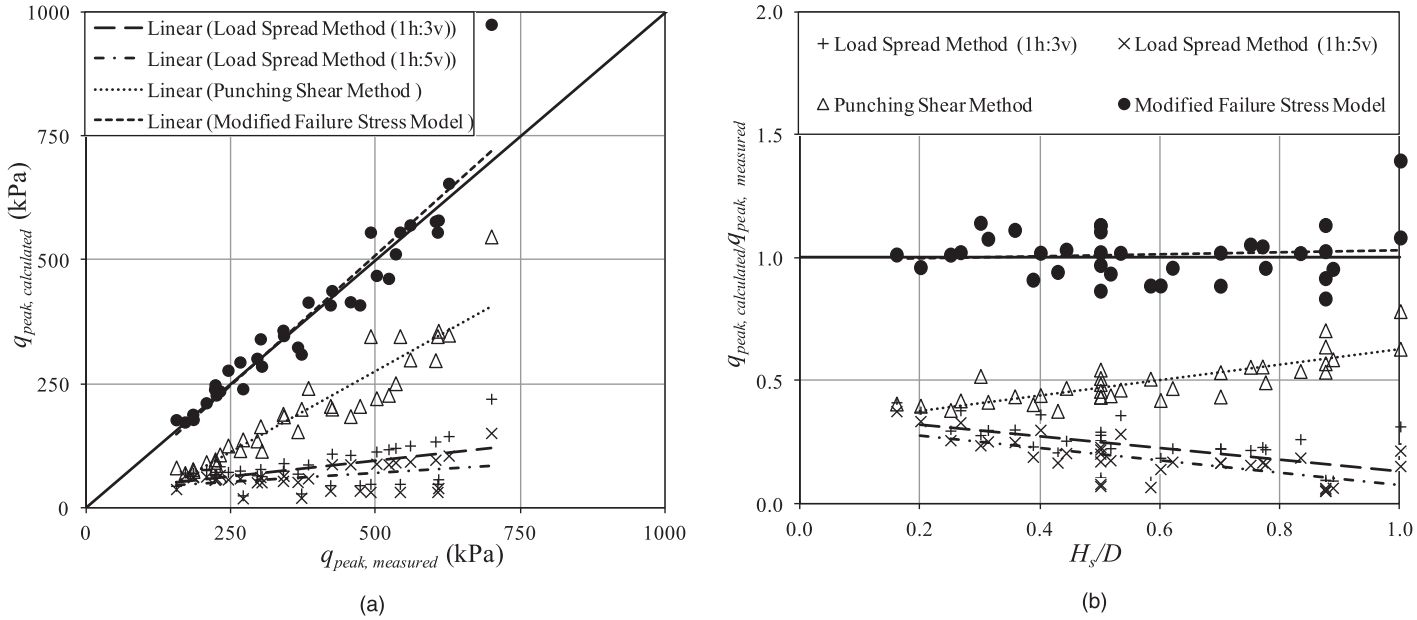

Fig. 11. Comparison of measured and calculated q_{peak} using ISO (2012) recommendations and modified and recalibrated failure-stress-dependent model (h = horizontal; v = vertical)

this validation were derived from tests with siliceous sand; consequently, Q in Eq. (4) was assumed to be 10 (Bolton 1986). The critical-state friction angle was taken as 31° for the sand used in the UWA tests (White et al. 2008) and 32° for the Toyoura sand used in the NUS tests (Jamiolkowski et al. 2003).

The performance of the modified model is compared with that of the primary model (based on the load-spread method) and alternative (based on the punching-shear method) recommendations of the ISO (2012). For each method, the measured and calculated peak penetration resistance predictions are presented with $q_{peak,calculated}$ against $q_{peak,measured}$ and $q_{peak,calculated}/q_{peak,measured}$ against H_s/D ratio, as shown in Fig. 11. A linear regression line is used in the $q_{peak,calculated}/q_{peak,measured}$ figure to identify any apparent trend in performance of the calculation with respect to H_s/D ratio. Table 3 provides a summary of key performance indicators such as mean, maximum, minimum, SD, and skew, where $\theta = \arctan(s)$, with s being the slope of the regression line.

For both the ISO (2012) primary and alternative recommendations, conservative predictions of q_{peak} are obtained, with most of the predicted peak penetration resistances less than 60% of the measured peak penetration resistances. The reason is that both methods ignore the properties of the sand: the load spread factor is

J. Geotech. Geoenviron. Eng., 2014, 140(2): 04013009

Table 3. Summary of Model Performance Indicators for Each of the Prediction Methods

Method	$q_{peak,calculated}/q_{peak,measured}$				
	Minimum	Maximum	Mean	SD	θ (degrees)
ISO (2012) recommendations (load-spread method with 1h:3v spread ratio)	0.07	0.41	0.23	0.09	−13.39
ISO (2012) recommendations (load-spread method with 1h:5v spread ratio)	0.05	0.37	0.18	0.09	−14.30
ISO (2012) alternative recommendations (punching-shear method)	0.38	0.78	0.50	0.09	17.66
Modified failure-stress-dependent model with recalibrated D_F	0.83	1.39	1.01	0.11	2.27

Note: h = horizontal; v = vertical.

not related to the sand properties in the primary recommendation, and the frictional resistance through the sand is expressed in terms of the normalized shear strength of the underlying clay layer in the alternative recommendation. The alternative recommendation made by ISO (2012) based on the punching-shear mechanism actually performs better than the primary recommendation based on the load-spread method. Referring back to Fig. 4 demonstrates the implication of this conservative prediction of q_{peak}. For both medium-loose and dense sands, such conservatism would lead to gross underestimation of the potential impact of both punch-through and rapid leg run because the depth over which the event may occur also would be underestimated. The skew angles presented in Fig. 11 and Table 3 demonstrate that the methods based on ISO (2012) recommendations exhibit significant bias in performance, with worsening predictions for larger H_s/D ratios for the load-spread method. This is so because at higher H_s/D ratios the thicker sand layer leads to the capacity of resistance generated by the sand being a larger proportion of q_{peak}. Hence, by ignoring the contribution of the sand layer in the load-spread method, the predictions worsen with increasing H_s/D ratio.

In contrast to the ISO (2012) recommendations, the modified failure-stress-dependent model with the recalibrated D_F provides an average of all the predictions of $q_{peak,calculated}/q_{peak,measured}$ of 1.01 and a SD of 0.11. All predictions, apart from Test NUS_F5 from Teh (2007), are within ±20% of the measured values. The significantly less skew with respect to H_s/D ratio for the predictions indicates that the modified failure-stress-dependent model is capable of accounting for changes in stratigraphy far more effectively than the ISO methods. This is so because the failure stress is highly dependent on sand thickness and foundation size, as demonstrated in Fig. 5, and the operative friction angle and angle of inclination of the inverted truncated-cone mechanism is related to the failure stress in the modified failure-stress-dependent model. By adopting the modified failure-stress-dependent model to improve the accuracy of estimation of q_{peak}, the uncertainty and risk associated with spudcan installation in sand overlying clay stratigraphies may be reduced.

Conclusions

Fifteen centrifuge tests have been conducted within a drum centrifuge to investigate spudcan foundation behavior on medium-loose sand overlying clay, representing the first comprehensive investigation of punch-through or rapid-leg-run potential for medium-loose sand overlying clay. The tests covered different prototype sand thicknesses in the range 3.2–6 m and spudcan diameters in the range 6–20 m, corresponding to H_s/D ratios of 0.16 to 1. This covers the range of practical interest for punch-through failure of jack-up platforms. These new data were combined with the data for spudcans penetrating dense sand overlying clay from Lee (2009) to allow recalibration of the modified failure-stress-dependent model. Interpretation of these data has led to the following conclusions:

1. The potential for catastrophic punch-through and rapid leg run of spudcans, already demonstrated for dense sand overlying clay, is also a potential problem for medium-loose sand overlying clay sites.
2. The depth of occurrence of q_{peak} has been further confirmed experimentally to be a function of H_s for the range of H_s/D ratios of practical interest. Coupling the depth of occurrence with accurate prediction of q_{peak} provides the first step in predicting the risk of punch-through failure for sand overlying clay sites.
3. The failure-stress-dependent model of Lee et al. (2013b) for predicting q_{peak} on sand overlying clay has been modified to account for mobilization-induced embedment. This modified mechanism has been used to derive an equation to describe q_{peak} in terms of the undisturbed sand thickness.
4. A new relationship has been proposed for D_F that is used to relate the stress at the failure surface to the average vertical stress in the modified failure-stress-dependent model. This provides improved prediction of q_{peak} over a larger range of sand-thickness-to-spudcan-diameter (H_s/D) ratios as well as sand relative densities. At this juncture, the new relationship has been calibrated and validated only for spudcan shapes similar to that tested here.
5. The modified failure-stress-dependent model, which is based on a kinematically admissible failure mechanism and accounts for the embedment depth caused by mobilization of q_{peak}, was shown to be capable of accurately predicting the peak penetration resistance q_{peak} for both loose and dense sand overlying clay.
6. The performance of the modified failure-stress-dependent model has been compared with the current recommended practice based on ISO (2012) primary and alternative recommendations, and it was demonstrated that the modified model provides more accurate prediction of q_{peak} with less bias in relation to H_s/D ratios for a wide range of dense and loose sand over clay sites.

In summary, when used to back-calculate centrifuge data, ISO (2012) q_{peak} prediction methods significantly underestimates the potential for punch-through during spudcan penetration on sand overlying clay. The modified failure-stress-dependent model improves the q_{peak} predictions, and its adoption for field conditions offshore has the potential to better predict the potential for punch-through or rapid-leg-run events during spudcan installation on sand overlying clay. This would significantly reduce the risk associated with operating jack-up platforms in offshore locations with sand overlying clay soil stratigraphy.

Acknowledgments

This work forms part of the activities of the Centre for Offshore Foundation Systems (COFS), which is supported by the Lloyd's Register Educational Trust as a Centre of Excellence and is now forming one of the primary nodes of the Australian Research Council

(ARC) Centre of Excellence in Geotechnical Science and Engineering. This project has received additional support from the Australia-China Natural Gas Technological Partnership Fund and the ARC Discovery program. The authors are grateful for this support and also to drum centrifuge technician Mr. Bart Thompson for his assistance during the experimental work and to Dr. Kok Kuen Lee for providing data on the original dense sand over clay experiments and for fruitful discussions regarding the work.

References

Bolton, M. D. (1986). "The strength and dilatancy of sands." *Geotechnique*, 36(1), 65–78.

Cheong, J. (2002). "Physical testing of jack-up footings on sand subjected to torsion." Honours thesis, Univ. of Western Australia, Perth, Australia.

Craig, W. H., and Chua, K. (1990). "Deep penetration of spud-can foundation on sand and clay." *Geotechnique*, 40(4), 541–556.

Drescher, A., and Detournay, E. (1993). "Limit load in translational failure mechanics for associative and non-associative materials." *Geotechnique*, 43(3), 443–456.

Finnie, I. M. S., and Randolph, M. F. (1994). "Punch-through and liquefaction induced failure of shallow foundations on calcareous sediments." *Proc., Int. Conf. on Behaviour of Offshore Structures*, Vol. 1, Pergamon, Boston, 217–230.

Hossain, M. S., and Safinus, S. (2012). "Perforation drilling and an innovative spudcan for mitigating punch-through in multilayered soils." *Proc., IADC/SPE 157640 Asia Pacific Drilling Technology Conf. and Exhibition*, Curran, New York, 1048–1059.

Houlsby, G. T., and Martin, C. M. (2003). "Undrained bearing capacity factors for conical footings on clay." *Geotechnique*, 53(5), 513–520.

ISO. (2012). "Petroleum and natural gas industries: Site-specific assessment of mobile offshore unit. 1: Jack-ups." *ISO 19905-1*, ISO/FDIS, Geneva.

Jamiolkowski, M. B., Lo Presti, D. C. F., and Manassero, M. (2003). "Evaluation of relative density and shear strength of sands from CPT and DMT." *Proc., Soil Behaviour and Soft Ground Construction (GSP 119)*, J. T. Germaine, T. C. Sheahan, and R. V. Whitman, eds., ASCE, Reston, VA, 201–238.

Koutsoftas, D., and Ladd, C. (1985). "Design strengths for an offshore clay." *J. Geotech. Engrg.*, 10.1061/(ASCE)0733-9410(1985)111:3(337), 337–355.

Lee, K. K. (2009). "Investigation of potential punch-through failure on sands overlaying clay soils." Ph.D. thesis, Univ. of Western Australia, Perth, Australia.

Lee, K. K., Cassidy, M. J., and Randolph, M. F. (2013a). "Bearing capacity on sand overlying clay soils: Experimental and finite element investigation of potential punch-through failure." *Geotechnique*, in press.

Lee, K. K., Randolph, M. F., and Cassidy, M. J. (2013b). "Bearing capacity on sand overlying clay soils: A simplified conceptual model." *Geotechnique*, in press.

Osborne, J. J., et al. (2008). "An introduction to InSafeJIP." *Proc., 2nd Jack-up Asia Conf. and Exhibition*, PetroMin, Singapore.

Stewart, D. P. (1992). "Lateral loading of piled bridge abutments due to embankment construction." Ph.D. thesis, Univ. of Western Australia, Perth, Australia.

Stewart, D. P., Boyle, R. S., and Randolph, M. F. (1998). "Experience with a new drum centrifuge." *Proc., Int. Conf. Centrifuge 98*, Vol. 1, Balkema, Leiden, Netherlands, 35–40.

Teh, K. L. (2007). "Punch-through of spudcan foundation in sand overlying clay." Ph.D. thesis, National Univ. of Singapore, Singapore.

Teh, K. L., Cassidy, M. J., Leung, C. F., Chow, Y. K., Randolph, M. F., and Quah, M. (2008). "Revealing the bearing capacity mechanisms of a penetrating spudcan through sand overlying clay." *Geotechnique*, 58(10), 793–804.

Teh, K. L., Leung, C. F., Cassidy, M. J., and Chow, Y. K. (2010). "Centrifuge model study of spudcan penetration in sand overlying clay." *Geotechnique*, 60(11), 825–842.

White, D. J., Take, W. A., and Bolton, M. D. (2003). "Soil deformation measurement using particle image velocimetry (PIV) and photogrammetry." *Geotechnique*, 53(7), 619–631.

White, D. J., Teh, K. L., Leung, C. F., and Chow, Y. K. (2008). "A comparison of the bearing capacity of flat and conical circular foundations on sand." *Geotechnique*, 58(10), 781–792.